

Communication

Dynamics of Gas Ionization by Laser Pulses with Different Envelope Shapes

Anna Emelina ^{1,*}, Ivan Laryushin ^{1,2}  and Alexander Romanov ^{1,2} 

¹ A.V. Gaponov-Grekhov Institute of Applied Physics (IAP RAS), 603950 Nizhny Novgorod, Russia; ilaryushin@mail.ru

² Department of Electrodynamics, Lobachevsky State University of Nizhny Novgorod, 603022 Nizhny Novgorod, Russia

* Correspondence: aemelina@ro.ru

Abstract: The properties of the dynamics of gas ionization under the action of femtosecond ionizing laser pulses with various envelope shapes are studied. It is shown that the duration of ionization in the saturation regime (at a high final degree of ionization) can either increase or decrease with an increase in the peak intensity of the ionizing pulse, depending on the shape of its envelope. We also determined the influence of the pulse shape on the spectrum of Brunel harmonics and the terahertz yield when two-color pulses are used.

Keywords: ionization dynamics; pulse envelope; terahertz generation; TDSE

1. Introduction

The processes of gas ionization by an intense laser pulse and the further interaction of free electrons with the field of the given pulse have been the subject of various studies over recent decades. There are a huge number of theoretical and experimental works devoted to the study of the dependence between the parameters of an ionizing pulse and the dynamics of oscillations in the plasma it creates [1–6]. Most often, the object of study is the characteristics of the pulse carrier, while the shape of its envelope is considered to be arbitrarily given. As a rule, Gaussian envelopes are used in semiclassical (photocurrent) calculations [5–9], while abruptly terminating envelopes can be used in quantum mechanical calculations to save computational resources [9–12], and for few-cycle pulses, additional requirements may be introduced [3,13].

By ionization dynamics we mean, first of all, the time dependence of the concentration of free electrons. The above-mentioned frequent lack of attention to the shape of the pulse envelope is predominantly due to the fact that when using low-intensity pulses, the vast majority of free electrons are generated near the maximum of the envelope, so any bell-shaped pulses will give practically indistinguishable results. Interest in the shape of the envelope arises in the case of high-intensity pulses that produce almost a complete ionization of the medium. In this case, the generation of free electrons shifts to the forefront of the pulse [7]. It is only during the active ionization that all the nonlinear (combinational/Brunel) components are generated in the plasma currents [8,9].

Previously, the dynamics of ionization, including the saturation regime, has been studied [7,8] for pulses with only a Gaussian envelope. Recently, a new method has been proposed for reconstructing the envelope of ultrashort pulses using ionization dynamics (TIPTOE [14,15]), from which our theory may be useful to develop into the region of longer pulses.

In this paper, we study in detail the differences in dynamics that arise when gases are ionized by moderately intense pulses with different envelope shapes in the tunneling regime. We show that in the ionization saturation regime, when the final degree of ionization is close to unity, the shape of the ionizing pulse envelope can determine the asymptotic



Citation: Emelina, A.; Laryushin, I.; Romanov, A. Dynamics of Gas Ionization by Laser Pulses with Different Envelope Shapes. *Photonics* **2023**, *10*, 499. <https://doi.org/10.3390/photonics10050499>

Received: 3 April 2023
Revised: 21 April 2023
Accepted: 24 April 2023
Published: 26 April 2023



Copyright: © 2023 by the authors. Licensee MDPI, Basel, Switzerland. This article is an open access article distributed under the terms and conditions of the Creative Commons Attribution (CC BY) license (<https://creativecommons.org/licenses/by/4.0/>).

behavior (increase or, conversely, decrease) of such characteristics as the ionization duration, spectral width of Brunel harmonics, or, for two-color pulses, the terahertz yield. Our semiclassical calculations and analysis are in a good agreement with the results of *ab initio* quantum-mechanical calculations.

2. Model

The equations that we used for analytical derivations and numerical calculations in wide range of parameters are based on the semiclassical approach (photocurrent model) [5,8,9]. To calculate the current density of free electrons generated by the laser field, we used the following system of equations:

$$\frac{\partial N}{\partial t} = (N_g - N)w(|\mathbf{E}|), \tag{1}$$

$$\frac{\partial \mathbf{j}}{\partial t} = \frac{e^2}{m} N \mathbf{E}, \tag{2}$$

with the initial conditions $N(t \rightarrow -\infty) = 0$ and $\mathbf{j}(t \rightarrow -\infty) = 0$. Here, N is free-electron density, N_g is the initial density of neutral particles, and we also define $\sigma(t) = N(t)/N_g$ as the degree of ionization. $w(|\mathbf{E}|)$ is the tunneling ionization probability per unit time under the action of an electric field \mathbf{E} , \mathbf{j} is the free-electron current density, e and m are electron charge and mass. The residual current density (RCD), which remains after the passage of the laser pulse and determines the amplitude of the following terahertz plasma oscillations, is $|\mathbf{j}(+\infty)|$. Such a residual current can be efficiently generated either by few-cycle single-color pulses [7,13,16] or by multicycle two-color pulses [2,8].

The electric field is given by

$$\mathbf{E} = \mathbf{x}f(t) \sum_k \mathcal{E}_k \cos(\omega_k t + \phi_k), \tag{3}$$

where \mathbf{x} is a unit vector along the x axis, $f(t)$ is a slow envelope normalized to unit maximum, $\mathcal{E}_k = \sqrt{8\pi I_k/c}$ is the maximum of the k -th component's amplitude, I_k is its peak intensity, and ω_k and ϕ_k are the central frequency and phase shift. In the calculations within this paper we either have a one-color field with ω_0 corresponding to wavelength $\lambda_0 = 800$ nm, or a two-color field with $\omega_1 = 2\omega_0$ and $\phi_0 = 0$. Our analytical calculations are performed under the assumption that the pulse is multicycle, $\omega_0 \gg 2\pi/\tau$ (τ is the laser pulse duration), and that the ionization regime is tunneling, with Keldysh parameter $\gamma = \omega_0/\omega_t \ll 1$ ($\omega_t = \mathcal{E}_0/\sqrt{2I_p}$ is the tunneling frequency, I_p is the ionization potential of an atom), but in numerical calculations we do not necessarily adhere to these limits.

The ionization probability per unit time for atomic hydrogen is given by Equation [17]:

$$w(|\mathbf{E}|) = 4\Omega_a \frac{E_a}{|\mathbf{E}|} \exp\left(-\frac{2E_a}{3|\mathbf{E}|} - \frac{12|\mathbf{E}|}{E_a}\right), \tag{4}$$

where E_a and Ω_a are the atomic field and frequency.

The obtained analytical results were also compared with the numerical solutions of the three-dimensional time-dependent Schrödinger equation (3D TDSE):

$$i\hbar \frac{\partial}{\partial t} \psi(\mathbf{r}, t) = \left[-\frac{\hbar^2}{2m} \nabla^2 - e\mathbf{r}\mathbf{E}(t) + V(r) \right] \psi(\mathbf{r}, t), \tag{5}$$

where $\psi(\mathbf{r}, t)$ is the electron wavefunction, \hbar is the reduced Plank constant, and $V(r) = -e^2/r$ is the potential energy of the electron in the Coulomb field of the nucleus of the hydrogen atom. The numerical 3D TDSE solution was performed similarly to [11] using an expansion of the wavefunction in spherical harmonics with the maximum orbital momentum $l_{\max} = 256$. The numerical integration was performed with time step $\Delta t = 0.02$ atomic units (a.u.) on the spatial grid of size $R_{\max} = r_{\max} + R_{\text{abs}}$ and radial step $\Delta r = 0.1$ a.u., where $r_{\max} = 200$ a.u. is the actual size of the calculation

region. $R_{\text{abs}} = 50$ a.u. is the width of the absorbing layer introduced near the boundary to suppress the unphysical reflection of the wavefunction. The absorbing layer is modeled by multihump imaginary potentials [18]. The generated radiation is characterized by Fourier spectrum $\mathbf{a}_\omega = \int \mathbf{a}(t)e^{i\omega t} dt$ of the atom dipole acceleration $\mathbf{a}(t)$, which determines the time derivative of the electron current density, $\partial \mathbf{j} / \partial t$:

$$\frac{\partial \mathbf{j}}{\partial t} = eN_g \mathbf{a}, \quad \mathbf{a} = \frac{1}{m} [e\mathbf{E} - \langle \psi | \nabla V | \psi \rangle]. \quad (6)$$

After the passage of the laser pulse, the current density \mathbf{j} is the sum of the constant component RCD of free electrons and the oscillating component \mathbf{j}_b of the electrons staying in the bound states. \mathbf{j}_b oscillates fast with time at frequencies determined by the transition energies between bound states. The RCD is found by subtracting \mathbf{j}_b from the total current density \mathbf{j} using time averaging.

3. Results and Discussion

Figure 1 illustrates the differences in the dynamics of ionization for two different shapes of the envelope of a single-color ionizing pulse. Both subplots show the time dependencies of the degree of gas ionization σ (the ratio of the ion concentration to the initial concentration of neutral atoms) for three different peak intensities of the ionizing pulse. As the intensity increases, the time $t_0 = \int_{-\infty}^{+\infty} t\sigma' dt$ (here, ' means time derivative $\sigma' = d\sigma/dt$) at which the most intense generation of free electrons happens shifts towards the forefront of the ionizing pulse. As for the duration of ionization $\tau_i = (\int_{-\infty}^{+\infty} (t - t_0)^2 \sigma' dt)^{0.5}$, in the case of the Gaussian shape (left subplot), it monotonously decreases, while with the Lorentzian shape (right subplot), it decreases from $I_0 = 2 \cdot 10^{14} \text{ W/cm}^2$ to $I_0 = 10^{15} \text{ W/cm}^2$ but then it grows back again (for each line on Figure 1 we indicated $t_0 \pm \tau_i$ with vertical dashed lines of the same color). In the following subsection, we will investigate this effect in more detail.

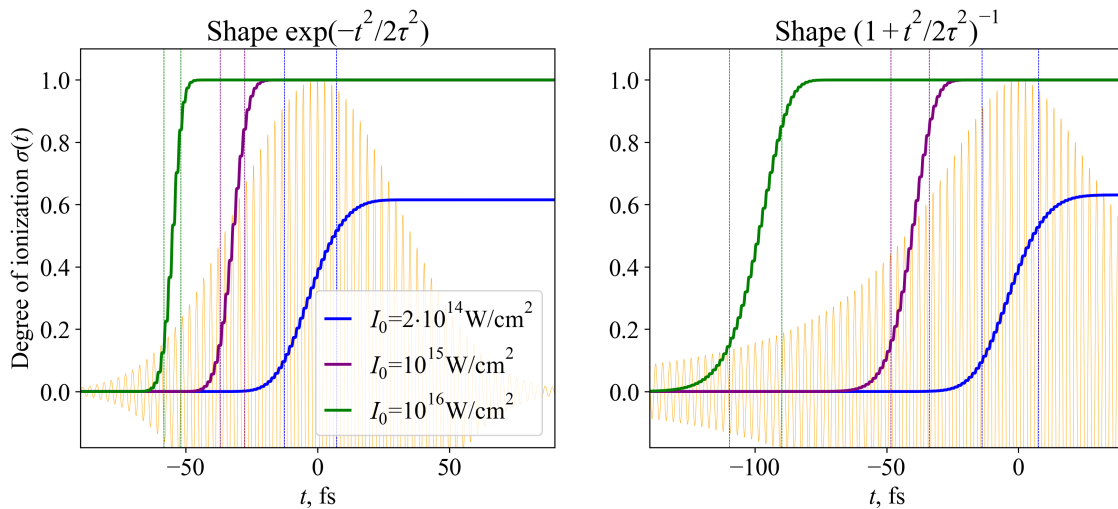


Figure 1. Dynamics of the degree of ionization of atomic hydrogen under the action of one-color laser pulses with Gaussian (left subplot) and Lorentzian (right subplot) envelope shapes with different peak intensities: $I_0 = 2 \cdot 10^{14} \text{ W/cm}^2$ for blue lines; $I_0 = 10^{15} \text{ W/cm}^2$ for purple lines; $I_0 = 10^{16} \text{ W/cm}^2$ for green lines. Pulse duration $\tau \approx 30$ fs (which corresponds to the full width at half maximum (FWHM) intensity duration $\tau_p = 50$ fs for the Gaussian pulse shape) and central wavelength is $\lambda_0 = 800$ nm. The thin red lines correspond to the normalized electric field of the laser pulse.

To describe the ionization dynamics in the case where the duration of the ionization significantly exceeds the period of the laser field, it is convenient to separate the fast and slow components of the free electron density and track the slow (period-averaged) component

$$\bar{N}(t) = N_g \left[1 - \exp\left(-\int_{-\infty}^t \bar{w}(t') dt'\right) \right], \tag{7}$$

where $\bar{w}(t) = \sqrt{2/\pi n_0} w(\mathcal{E}_0 f(t))$ is the period-averaged ionization rate (which is a function of the amplitude of the laser field, not its instantaneous value) and $n_0(E) = w'(E)E/w(E)$ is the effective exponent of ionization probability (which is the order of nonlinearity in this system [8]).

3.1. Analytical Solutions

In this subsection, we investigate the relationship between the parameters t_0 and τ_i of the ionization process and the shape of the envelope of single-color laser pulses. At low finite degrees of ionization, one can put $(N_g - N) \approx N_g$ in Equation (1), in which case we have $t_0 = 0, \tau_i \approx \tau/\sqrt{n_0}$ [7,8].

Let us consider a more general case, where the final degree of ionization is arbitrary. As can be seen from Figure 1, $d\bar{N}/dt$ is also a bell-shaped peak. So, the condition for the maximum of $d\bar{N}/dt$ can be written as

$$\bar{N}'' = (N_g - \bar{N})(\bar{w}' - \bar{w}^2) = 0. \tag{8}$$

Denote $E_0(t) = \mathcal{E}_0 f(t)$, and by substituting $\bar{w}'(E_0(t)) \approx n_0 \bar{w} f' / f$ into Equation (8) we can rewrite the condition on t_0 :

$$\frac{f'}{f}(t_0) = \frac{\bar{w}}{n_0}(E_0(t_0)). \tag{9}$$

The left side of the expression (9) does not depend on the peak intensity of the main component of the ionizing pulse, only on the shape of the envelope. The duration of ionization can be approximated as

$$\tau_i \approx \left(-\frac{\bar{N}'''(t_0)}{\bar{N}'(t_0)}\right)^{-1/2} = \left(\frac{n_0 f''}{f} - \frac{n_0^2 f'^2}{f^2}\right)^{-1/2}. \tag{10}$$

In this paper we consider the three main types of envelopes:

$$f_0(t) = \exp\left(-\frac{t^2}{2\tau^2}\right); \tag{11}$$

$$f_1(t) = 1/\cosh\left(\frac{t}{\tau}\right); \tag{12}$$

$$f_2(t) = \left(1 + \frac{t^2}{2\tau^2}\right)^{-1}. \tag{13}$$

Here, $\tau = [-f''(t = 0)/f]^{-1/2}$ is the characteristic duration of the ionizing pulse in all three cases; the intensity FWHM durations τ_p actually slightly differ with different envelopes, for example, for FWHM duration $\tau_p = 30$ fs, we obtain $\tau = \tau_p/\sqrt{4 \log 2} \approx 18$ fs for the Gaussian pulse shape (11), $\tau = \tau_p/[2 \operatorname{arccosh} \sqrt{2}] \approx 17$ fs for the \cosh^{-1} pulse shape (12), and $\tau = \tau_p/[2^{3/2} \sqrt{\sqrt{2} - 1}] \approx 16.5$ fs for the Lorentzian shape (13). However, the shapes near the maxima of the envelope are similar for all three. As can also be seen from Figure 2 in the next subsection, $-t_0$ grows monotonically with I_0 and the specific dependence is determined by the shape of the pulse envelope. In [7], there was an approximation proposed for t_0 in the case of the Gaussian envelope, through the Lambert W function. Asymptotically, its behavior can be described by denoting by $\zeta(1/t)$ the function

inverse to $\bar{w}(E)/n_0(E)$ (the function ξ has the physical dimension of the electric field) as follows:

$$-t_0/\tau = \begin{cases} \ln(\mathcal{E}_0/\xi(1/\tau)), & \mathcal{E}_0 \gg \xi(1/\tau) \\ \tau\bar{w}(\mathcal{E}_0)/n_0(\mathcal{E}_0), & \mathcal{E}_0 \ll \xi(1/\tau). \end{cases} \tag{14}$$

If we follow the approximation procedure proposed in Ref. [7], the expression for t_0 will not differ for different pulse shapes. However, in reality, the dependencies of t_0 on I_0 differ somewhat for different envelopes, while exact expressions cannot be obtained analytically since they are roots of transcendental equations. At the same time, the most interesting properties of ionization dynamics can be analyzed even without obtaining this expression, if we simply use t_0 as some monotonic function of I_0 . More specifically, we can express in terms of t_0 the duration of ionization τ_i and the average probability of ionization $\bar{w}(t_0)$.

For $f = f_0$, the following expressions are obtained:

$$\bar{w}(t_0) = -n_0 t_0 / \tau^2; \quad \tau_i = \left(\frac{n_0}{\tau^2} + \frac{n_0^2 t_0^2}{\tau^4} \right)^{-1/2}. \tag{15}$$

With an increase in t_0 (which corresponds to an increase in I_0), the duration of ionization decreases. For $f = f_1$ we obtain

$$\bar{w}(t_0) = n_0 \tanh(-t_0/\tau) / \tau; \quad \tau_i = \left(\frac{n_0}{\tau^2} + \frac{n_0^2 \tanh^2(t_0/\tau)}{\tau^2} \right)^{-1/2}. \tag{16}$$

In this case, the duration of ionization becomes constant with increasing t_0 (\tanh is hyperbolic tangent). For $f = f_2$ we obtain

$$\bar{w}(t_0) = \frac{2n_0 t_0}{2\tau^2 + t_0^2}; \quad \tau_i = \left(\frac{n_0}{\tau^2} + \frac{n_0^2 t_0^2}{\tau^4} \right)^{-1/2} \left(1 + \frac{t_0^2}{2\tau^2} \right). \tag{17}$$

In this case, as t_0 increases, the duration of ionization increases.

The characteristics of the ionization dynamics calculated above are related to more understandable measurable quantities. The most direct connection here exists with the generation of terahertz radiation under the action of two-color ionizing pulses, described in article [8], which shows that if the intensity of the second harmonic in a two-color pulse is low (1% or less), then the averaged ionization dynamics is almost completely determined by the main field and is similar to that in a one-color field. However, all analysis and calculations were previously performed only for Gaussian envelopes, and using the regularities obtained in the current work, these results can be generalized. Formulas (15)–(17) in all cases lead to the same relation for $t_0 \gg \tau/n_0$:

$$\bar{w}(t_0) \sim \tau_i^{-1}. \tag{18}$$

RCD at a large t_0 has the proportionality $|j(t = +\infty)| \sim E_0(t_0)\bar{w}(E_0(t_0))\tau_i \sim E_0(t_0)$ [8], and since \bar{w} is a monotonic function of the field strength, $E_0(t_0)$ has a similar behavior (increase or decrease in dependence of t_0). In other words, when using envelopes of an ionizing laser pulse that decay faster than exponentially, the energy of the generated terahertz pulse will continue to slowly increase with increasing peak intensity above the threshold corresponding to full ionization, and vice versa, when using slowly decaying envelopes, such as the Lorentzian (13), the energy will decrease with increasing intensity.

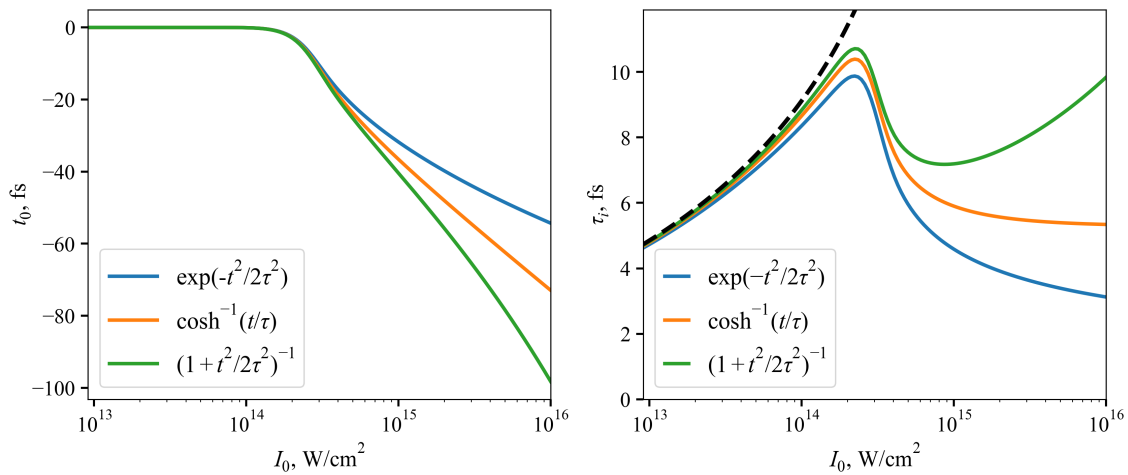


Figure 2. (Left subplot) Dependence of the time corresponding to the most intense generation of free electrons t_0 on the peak intensity of the one-color laser field I_0 for the three different envelope shapes of ionizing pulses. The blue line corresponds to the Gaussian pulse shape given by the expression (11), the orange line corresponds to the \cosh^{-1} pulse shape given by the expression (12), and the green line corresponds to the Lorentzian pulse shape given by the expression (13). (Right subplot) Dependence of ionization duration τ_i on the intensity of the one-color field I_0 . The dotted line corresponds to $\tau / \sqrt{n_0(\mathcal{E}_0)}$. Pulse duration is $\tau = 30$ fs (which corresponds to FWHM $\tau_p \approx 50$ fs for the Gaussian pulse shape), central wavelengths are 800 nm.

3.2. Numerical Calculations

We performed both semiclassical and quantum-mechanical numerical calculations to validate the developed analytical model. Within the framework of the quantum-mechanical approach, the concentration of free electrons does not have a clear definition. Usually, this definition is introduced in terms of the norm of the wave function outside a sphere with a radius large enough to exclude most of the bound states of the atom. In this case, in contrast to the semiclassical approach, the concentration of free electrons does not necessarily increase monotonically with time, so the studied characteristics also do not necessarily have the same values as in the semiclassical/photocurrent model. However, our analytical equations also predict the dependency of the terahertz output value for various two-color pulse envelope shapes, and this characteristic is more specifically defined for TDSE solutions; this is how we can check the validity of both our analytical approximations and the semiclassical model itself for a more rigorous approach.

The left subplot of Figure 2 shows the dependences of t_0 on I_0 for three different pulse shapes, obtained from semiclassical calculations. Qualitatively, these dependences are arranged in the same way, but there is a certain quantitative difference. In this case, if we observe the ionization duration τ_i (right subplot of Figure 2), then qualitative differences appear here in accordance with Equations (15)–(17). As long as the degree of ionization is small (for hydrogen in a single-color field, this corresponds to intensities $I_0 < 10^{14}$ W/cm²), the shape of the tail of the ionizing pulse does not play any role in the ionization dynamics, because with the same τ parameters, all three forms have the same shape near the maximum, where almost all ionization occurs. Then, at moderate intensities $10^{14} < I_0 < 5 \cdot 10^{14}$ W/cm², while $t_0 < \tau$, the behavior of τ_i is still similar for all the three shapes, since the differences in the shapes of the envelopes in the region of active ionization are still small; however, all three dependences deviate from a simple analytical curve. Additionally, already at high intensities, $I_0 > 5 \cdot 10^{14}$ W/cm², we observe different asymptotic behaviors of the ionization duration in accordance with the theory obtained.

A similar difference, which also coincides with the predictions of the analytical model, is also observed in the dependence of the value of the field amplitude $E_0(t_0)$ on the intensity of the one-color field I_0 (Figure 3, left subplot). All these effects combined are reflected in

the dependences of RCD on I_0 for different pulse shapes, obtained from both semiclassical and the 3D TDSE solutions, which are shown on the right subplot of Figure 3. In this case, we performed calculations for a sufficiently high intensity of the second harmonic (the ratio of the amplitudes of the components is 0.3, and the ionization dynamics then ceases to depend only on the fundamental field). Nevertheless, the correspondence between the dependences on the two subplots in Figure 3 is visual at high intensities $I_0 > 5 \cdot 10^{14} \text{ W/cm}^2$. Small fluctuations of quantum-mechanical solutions relative to semiclassical ones can be associated with a slight difference between the ionization probability and the analytical Formula (4), which does not take into account a number of effects such as the dependence of the energy of the atomic level on intensity due to the dynamic Stark shift, and does not describe ionization through bound states and multiphoton ionization, which have a quasi-stepwise dependence on the intensity and wavelength of the laser field due to the opening–closing of multiphoton ionization channels. However, in general, we see the correct dependencies on the TDSE solutions, corresponding to the proposed theory. In addition to the three basic envelope shapes (11)–(13), Figure 3 also shows TDSE calculations with a frequently used [9–12] shape $f(t) = \cos^2(\pi t/T)$, saving computational time, which is a valuable resource for 3D TDSE. As can be seen, in the region of high intensities $\gtrsim 10^{15} \text{ W/cm}^2$, this shape gives an increase in the RCD even greater than that of the Gaussian, since it decreases even faster.

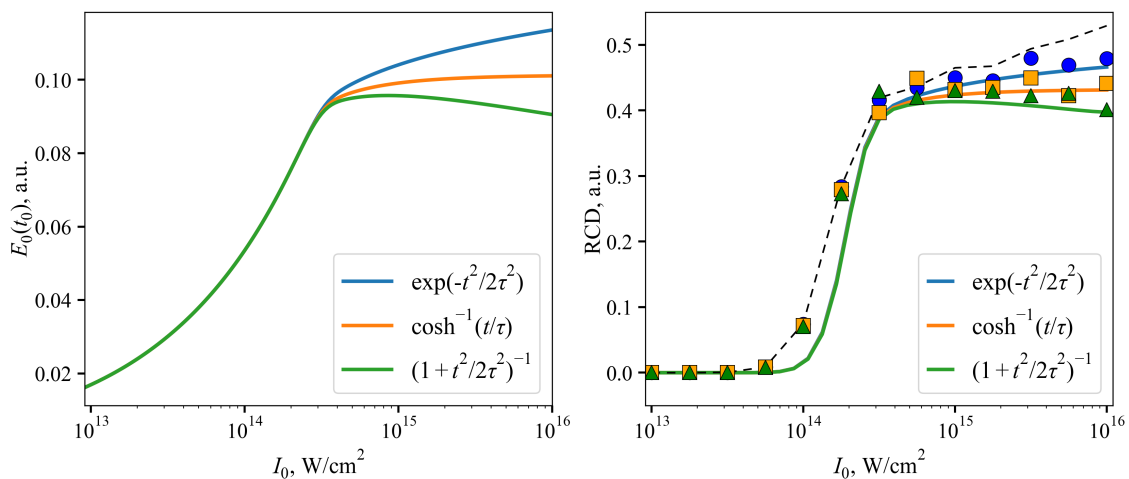


Figure 3. (Left subplot) Dependence of $E_0(t_0)$ on the peak intensity of the one-color field I_0 for the three envelope shapes of ionizing pulses. Pulse durations $\tau = 18 \text{ fs}$ and central wavelengths are 800 nm . (Right subplot) Dependence of residual current density $|\mathbf{j}(t = +\infty)|$ (proportional to the amplitude of the subsequent terahertz plasma oscillations) on intensity I_0 for two-color pulses with a 9% addition of second harmonic $I_1 = 0.09I_0$. FWHM duration of all pulses is $\tau_p = 30 \text{ fs}$, central wavelengths are 800 nm , phase ϕ_1 is optimized at every point and corresponds to the maximum RCD generation. Solid lines with different colors correspond to the semiclassical calculations with the same envelope shapes as on the left subplot. Blue circles, orange squares, and green triangles are TDSE results for Gaussian, \cosh^{-1} , and Lorentzian pulse shapes, respectively. Black dashed line is a TDSE result for abruptly terminating envelope $f(t) = \cos^2(\pi t/T)$ for $-T/2 < t < T/2$, where $T = 82.4 \text{ fs}$ is the pulse duration corresponding to FWHM $\tau_p = 30 \text{ fs}$.

3.3. Presence of a Prepulse

Earlier in the article, the effects associated with smooth pulse envelopes were studied in detail. In reality, measurements of pulse envelopes rarely show any smooth front shape far from the maximum of the envelope [15,19,20]. In this subsection, we consider the

dynamics of ionization under the action of a pulse with a weaker prepulse, the envelope of which is given by

$$f_p(t) = \exp\left(-\frac{t^2}{2\tau^2}\right) + \alpha \exp\left(-\frac{(t + \Delta T)^2}{2\tau^2}\right), \quad (19)$$

where ΔT is the time shift between the maxima of the pulse and the prepulse, and α^2 is the ratio between the peak intensities of the prepulse and the main pulse. The left subplot in Figure 4 shows the ionization dynamics for a pulse with $\alpha = 0.5$ and $\Delta T = 100$ fs. When the value $I_0 \approx 10^{15}$ W/cm² is reached, the time profile of the derivative of the degree of ionization σ' becomes two-peak, as can be seen from the figure. Accordingly, the envelopes of the Brunel harmonics acquire the same shape, and an interference structure with period $\approx 2\pi/\Delta T$ appears in their spectrum. The right panel of Figure 4 shows the dj/dt squared spectrum normalized to the maximum value near the third harmonic, with a varying peak intensity of the laser pulse (19). The interference fringes become most contrasting at an intensity $I_0 \approx 10^{15}$ W/cm², at which two ionization peaks produce an equal number of free electrons (the degree of ionization increases by 0.5 in each). In addition, this picture also makes it possible to reconstruct the dependence of the ionization duration, which, in the case of a single σ' peak, is inversely proportional to the spectral linewidth of Brunel harmonics.

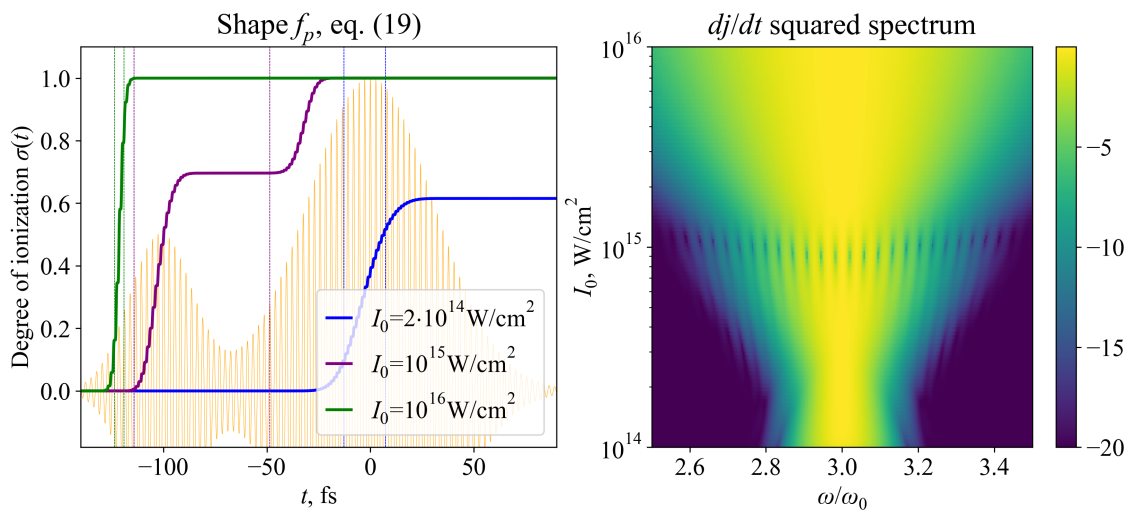


Figure 4. Dynamics of the degree of ionization of atomic hydrogen under the action of laser pulses with shape given by Equation (19). Lines differ by peak intensities: $I_0 = 2 \cdot 10^{14}$ W/cm² for blue lines; $I_0 = 10^{15}$ W/cm² for purple lines; and $I_0 = 10^{16}$ W/cm² for green lines. Pulse duration $\tau = 30$ fs, $\alpha = 0.5$ and $\Delta T = 100$ fs, central wavelength is 800 nm. The thin red lines correspond to the normalized electric field of the laser pulse. **(Right subplot)** Dependence of dj/dt normalized squared spectrum (in logarithmic scale) near the third harmonic on the peak intensity of the ionizing dual-max pulse with shape (19). The noise is suppressed at the e^{-20} level.

Overall, though the real envelope shapes can be much more complicated, we have demonstrated the possibility of relating the measurable characteristics of the ionization dynamics, in the case when it occurs over more than one field period, to the characteristics of envelopes, including those with nonmonotonic fronts. A similar analysis can be performed for more complex shapes, but it is reasonable to carry out such studies focusing on specific practical problems, the solution of which will be the goal of future work.

4. Conclusions

We have studied in detail the dynamics of free electron generation under the action of ionizing femtosecond laser pulses with various envelope shapes. The main parameters characterizing the dynamics are the duration of ionization and the time shift of the

maximum rate of increase in the concentration of free electrons. At low intensities, the dynamics is almost similar, but when the ionization is saturated (which corresponds to the intensities $\gtrsim 4 \cdot 10^{14}$ W/cm² at the ionization potential of 13.6 eV), the shape of the envelope begins to play a significant role. The duration of ionization can either grow logarithmically (for a Gaussian envelope), decrease (for a Lorentzian envelope), or become constant (for envelopes specified by an inverse hyperbolic cosine) with the growth in the peak intensity of the pulse. Our theoretical findings may be useful for the improvement of the TIPTOE method for measuring pulse envelopes [14,15]. We also show that the shape of the envelope determines the dependence of the terahertz yield on the peak intensity of a two-color pulse with a fixed intensity ratio between the first and the second harmonic, and our analytical results based on the simple photocurrent model are in a good agreement with the solutions of 3D TDSE.

Author Contributions: Analytical model (A.E. and I.L.), numerical calculations (A.E. and A.R.). All authors have read and agreed to the published version of the manuscript.

Funding: This research was funded by the Russian Science Foundation (Grant No. 21-72-00034).

Data Availability Statement: The data underlying the results presented in this paper are not publicly available at this time, but may be obtained from the authors upon reasonable request.

Conflicts of Interest: The authors declare no conflicts of interest.

Abbreviations

The following abbreviations are used in this manuscript:

RCD	residual current density
TDSE	time-dependent Schrödinger equation
FWHM	full width at half maximum
TIPTOE	tunneling ionization with a perturbation for the time-domain observation of an electric field

References

1. Brunel, F. Harmonic generation due to plasma effects in a gas undergoing multiphoton ionization in the high-intensity limit. *J. Opt. Soc. Am. B* **1990**, *7*, 521–526. [[CrossRef](#)]
2. Cook, D.; Hochstrasser, R. Intense terahertz pulses by four-wave rectification in air. *Opt. Lett.* **2000**, *25*, 1210–1212. [[CrossRef](#)] [[PubMed](#)]
3. Geissler, M.; Tempea, G.; Scrinzi, A.; Schnürer, M.; Krausz, F.; Brabec, T. Light propagation in field-ionizing media: Extreme nonlinear optics. *Phys. Rev. Lett.* **1999**, *83*, 2930. [[CrossRef](#)]
4. Jang, D.; Schwartz, R.M.; Woodbury, D.; Griff-McMahon, J.; Younis, A.H.; Milchberg, H.M.; Kim, K.Y. Efficient terahertz and Brunel harmonic generation from air plasma via mid-infrared coherent control. *Optica* **2019**, *6*, 1338–1341. [[CrossRef](#)]
5. González de Alaiza Martínez, P.; Babushkin, I.; Bergé, L.; Skupin, S.; Cabrera-Granado, E.; Köhler, C.; Morgner, U.; Husakou, A.; Herrmann, J. Boosting terahertz generation in laser-field ionized gases using a sawtooth wave shape. *Phys. Rev. Lett.* **2015**, *114*, 183901. [[CrossRef](#)] [[PubMed](#)]
6. Voronin, A.; Zheltikov, A. Laser-driven tunneling photocurrent as a source of midinfrared to microwave multidecade supercontinua yoked to high-order harmonics. *Phys. Rev. A* **2020**, *101*, 043813. [[CrossRef](#)]
7. Silaev, A.A.; Vvedenskii, N.V. Analytical description of generation of the residual current density in the plasma produced by a few-cycle laser pulse. *Phys. Plasmas* **2015**, *22*, 053103. [[CrossRef](#)]
8. Vvedenskii, N.V.; Kostin, V.A.; Laryushin, I.D.; Silaev, A.A. Excitation of low-frequency residual currents at combination frequencies of an ionising two-colour laser pulse. *Quantum Electron.* **2016**, *46*, 419. [[CrossRef](#)]
9. Laryushin, I.; Romanov, A. Analysis of Combination Frequencies Arising from the Ionization of Gases by Multicolor Femtosecond Pulses. *Photonics* **2022**, *9*, 444. [[CrossRef](#)]
10. Emelina, A.; Emelin, M.Y.; Ryabikin, M.Y. Wavelength scaling laws for high-order harmonic yield from atoms driven by mid- and long-wave infrared laser fields. *JOSA B* **2019**, *36*, 3236–3245. [[CrossRef](#)]
11. Romanov, A.A.; Silaev, A.A.; Sarantseva, T.S.; Frolov, M.V.; Vvedenskii, N.V. Study of high-order harmonic generation in xenon based on time-dependent density-functional theory. *New J. Phys.* **2021**, *23*, 043014. [[CrossRef](#)]
12. Emelina, A.; Emelin, M.Y.; Ryabikin, M.Y. Subattosecond keV beats of the high-harmonic x-ray field produced with few-cycle mid-IR laser pulses: Magnetic-field effects. *Phys. Rev. A* **2016**, *93*, 043802. [[CrossRef](#)]
13. Silaev, A.A.; Vvedenskii, N.V. Residual-current excitation in plasmas produced by few-cycle laser pulses. *Phys. Rev. Lett.* **2009**, *102*, 115005. [[CrossRef](#)] [[PubMed](#)]

14. Park, S.B.; Kim, K.; Cho, W.; Hwang, S.I.; Ivanov, I.; Nam, C.H.; Kim, K.T. Direct sampling of a light wave in air. *Optica* **2018**, *5*, 402–408. [[CrossRef](#)]
15. Cho, W.; Hwang, S.I.; Nam, C.H.; Bionta, M.R.; Lassonde, P.; Schmidt, B.E.; Ibrahim, H.; Légaré, F.; Kim, K.T. Temporal characterization of femtosecond laser pulses using tunneling ionization in the UV, visible, and mid-IR ranges. *Sci. Rep.* **2019**, *9*, 16067. [[CrossRef](#)] [[PubMed](#)]
16. Zhou, Z.; Zhang, D.; Liu, J.; Zhao, Z.; Lin, C.D. Searching for optimal THz generation through calculations of the asymmetry of photoelectron momentum distributions by an improved strong-field-approximation method. *Phys. Rev. A* **2023**, *107*, 013106. [[CrossRef](#)]
17. Tong, X.M.; Lin, C.D. Empirical formula for static field ionization rates of atoms and molecules by lasers in the barrier-suppression regime. *J. Phys. B At. Mol. Opt. Phys.* **2005**, *38*, 2593. [[CrossRef](#)]
18. Silaev, A.A.; Romanov, A.A.; Vvedenskii, N.V. Multi-hump potentials for efficient wave absorption in the numerical solution of the time-dependent Schrödinger equation. *J. Phys. B At. Mol. Opt. Phys.* **2018**, *51*, 065005. [[CrossRef](#)]
19. Täschler, P.; Bertrand, M.; Schneider, B.; Singleton, M.; Jouy, P.; Kapsalidis, F.; Beck, M.; Faist, J. Femtosecond pulses from a mid-infrared quantum cascade laser. *Nat. Photonics* **2021**, *15*, 919–924. [[CrossRef](#)] [[PubMed](#)]
20. Rampur, A.; Spangenberg, D.M.; Stepniewski, G.; Dobrakowski, D.; Tarnowski, K.; Stefańska, K.; Paździor, A.; Mergo, P.; Martynkien, T.; Feurer, T.; et al. Temporal fine structure of all-normal dispersion fiber supercontinuum pulses caused by non-ideal pump pulse shapes. *Opt. Express* **2020**, *28*, 16579–16593. [[CrossRef](#)] [[PubMed](#)]

Disclaimer/Publisher’s Note: The statements, opinions and data contained in all publications are solely those of the individual author(s) and contributor(s) and not of MDPI and/or the editor(s). MDPI and/or the editor(s) disclaim responsibility for any injury to people or property resulting from any ideas, methods, instructions or products referred to in the content.